Vision, Modeling, and Visualization (2021)
B. Andres, M. Campen, and M. Sedlmair (Eds.)

Refinable multi-sided caps for bi-quadratic splines

Kęstutis. Karčiauskas[1] and Jörg Peters[2]

[1] Vilnius University [2] University of Florida

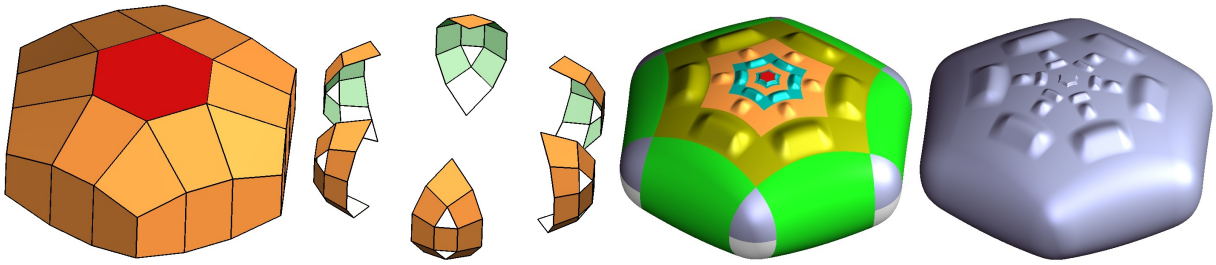

(a) mesh (b) adjacent $n = 3$ (c) locally embossed

Figure 1: *Design starting with (a) two hexagonal configurations (two $n = 6$ 'DS-nets' connected by one ring of quads). There are $2 \times n$ vertices of valence 3 from which tensor-product spline refinement creates (b) overlapping $n = 3$ DS-net pairs after one refinement. (c) C^1 smooth design features on the transition and contracting rings. The plain shading emphasizes overall smoothness between bi-quadratic patches, the bronze transition ring, a sequence of contracting rings (orange and blue) and a final curved and smoothly-joined tiny cap and the local embossing at different scales illustrates refinability.*

Abstract

Subdivision surfaces based on bi-quadratic splines have a control net, the DS-net, whose irregularities are n-sided facets. To date their limit shape is poor due to a small footprint of the refinement rules and the difficulty of controlling shape at the center irregularity. By contrast, a control net where vertices are surrounded by n quadrilateral faces, a CC-net, admits higher-quality subdivision and finite polynomial constructions. It would therefore be convenient to leverage these constructions to fill holes in a C^1 bi-quadratic spline complex.

In principle the switch in layout from a control net with central n-sided facet to one with a central irregular point is easy: just apply one step of Catmull-Clark refinement. The challenge, however, is to define the transition between the bi-quadratic bulk and the n-sided cap construction to be of sufficiently good shape to not destroy the advantage of higher-quality algorithms. This challenge is addressed here by explicit formulas for conversion from a DS-net to a CC-net.

1. Motivation

Polyhedral nets where an n-sided face is surrounded by n sectors of quadrilaterals, offer few – if any – surface construction options of good quality. The classic algorithm associated with n-sided facets surrounded by quads, Doo-Sabin subdivision [DS78], suffers from flat spots. Augmented Subdivision [KP15b] goes some way towards countering the flatness of bi-quadratic subdivision surfaces. However, Augmented Subdivision, too, fails at closer inspection of its highlight lines as illustrated in Fig. 2 c: while kinks in the highlight lines are natural for bi-2 C^1 splines, repeating kinks ad infinitum is not acceptable. One could apply Catmull-Clark subdivision [CC78] to the whole net, thereby increasing the degree of the surface everywhere. But this, too, fails the test of good shape, due to oscillating highlight lines [BC94], see Fig. 2 d: good shape means that the highlight lines flow as uniformly as possible. The bi-quartic (bi-4) construction [KP21] Fig. 2 e yields a uniform flow but lacks easy refinability for hierarchical geometric manipulation or engineering analysis. The features crossing the sectors in Fig. 1 c would be challenging if not impossible to graft onto a G^1 surface constructed according to the bi-4 construction in [KP21]. For that reason [KP21] presented an alternative: a few subdivision surface rings closed by a small cap, all following an initially-constructed guide surface. Due to the guide surface, the alternative is not easily implemented. By contrast, the construction of this paper is easy to implement based on explicit formulas and generates surfaces of quality adequate for bi-quadratic splines.

DOI: 10.2312/vmv.20211371

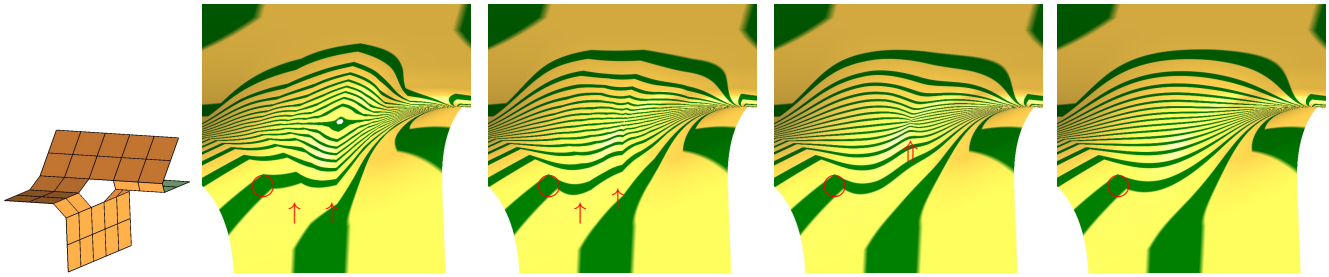

(a) Hexagonal face (b) Doo-Sabin (c) Augmented (d) Catmull-Clark (e) [KP21]

Figure 2: *Polyhedral net merging four planes with a central hexagonal face. Current surface constructions either fail to produce good shape (b,c,d) or lack refinability (e). Note that all the ○-circled kink is part of the surrounding C^1 bi-2 surface, but the repetition of the kinks, marked by ↑, is due to the subdivision algorithm. ⇑ points to the pinching artifact of [CC78].*

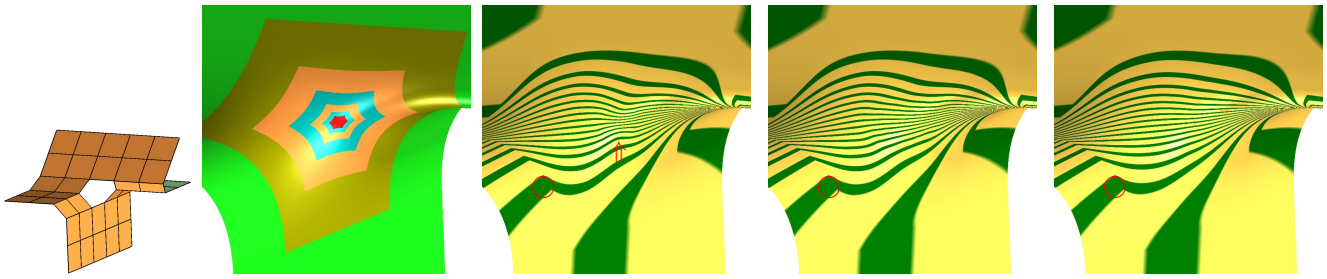

(a) Hexagonal face (b) surface rings (c) [CC78]-hybrid (d) [MM18]-hybrid (e) [KP19]-hybrid

Figure 3: *Refinable, yet finite, 'hybrid' surface constructions of the same input as for Fig. 2 (b) Hybrid structure: first a transition surface ring (bronze), then a few subdivision rings and finally a tiny cap. Rings from (c) Catmull Clark subdivision (degree bi-3) (d) Curvature-bounded subdivision [MM18] (degree bi-3). (e) Guided subdivision (degree bi-4). Option (e) requires fewer rings since this subdivision can be accelerated without loss of good highlight line distribution. (The kink in the circle ○ is due to the surrounding C^1 bi-2 surface).*

The contributions of this paper are

- to provide *refinable* multi-sided caps with good highlight line distribution
- by constructing a *fair transition* from the regular bi-2 splines to constructions usually reserved for filling multi-sided regions in a bi-3 C^2 spline surface;
- to provide the option of polynomial surfaces with *finitely* many pieces by completing the surface by a tiny bi-cubic cap after placing a few subdivision rings – based on explicit formulas rather than a guide surface.
- Notably the transitions between the surface rings are *parametrically* C^1 (or C^2) so that refinability is straightforward in the bulk of the surface.

The few subdivision rings, see Fig. 3 b, can be chosen as simple as standard Catmull-Clark subdivision, see Fig. 3 c, as curvature-bounded subdivision, see Fig. 3 d, or as complex as guided subdivision, where a sequence of C^1 bi-4 rings follow a guide surface, see Fig. 3 e. Their highlight line distributions [BC94] indicate improved shape of the multi-sided surface cap starting with the bronze ring in return for increased complexity and polynomial degree. Given that the surrounding bi-quadratic (bi-2) spline already introduces shape deficiencies, see ◯ in Fig. 3 , [MM18] provides a good trade-off for using simple rules and suitable quality. Of course all subdivision algorithms can also be applied to the limit, doing away with the tiny cap.

The key is therefore the transition from the bi-2 splines to higher-degree cap constructions (or, with the notation explained in Section 2, from DS-nets to CC-nets). Combinatorially this is trivial, but as Fig. 13 e clearly illustrates, naively applying one local Catmull-Clark refinement step yields unacceptable shape.

Overview After reviewing related literature in Section 1.1, Section 2 defines the critical bi-2 to bi-3 transition. The detailed motivation and derivation in Section 2.2 is summarized in a set of explicit formulas (3), (4) for implementation. Section 2.4 constructs the smooth bi-3 transition surface ring that connects to the bi-2 data on the outside and a multi-sided cap on the inside. Section 3 justifies the algorithmic choices via examples.

1.1. Related work

Grid-like meshes can be interpreted as control nets of bi-cubic (bi-3) splines, or C^1 biquadratic (bi-2) splines of lower quality but still sufficient for many applications. To fill multi-sided holes, the spline refinement rules have been generalized to Catmull-Clark subdivision [CC78] respectively Doo-Sabin subdivision [DS78]. Both

suffer from artifacts: Catmull-Clark surfaces from pinched highlight lines and hyperbolic limits even for convex control polyhedra [KPR04]. By adjusting subdivision weights, [CADS09,MM18] improve the behaviour at the central limit extraordinary point, [LFS16] directly prescribe parts of the eigenstructure while [KP07, TSHH17] prescribe the limit by (parts of) a guide surface. All these approaches remove artifacts, at the cost of a more complex algorithm than Catmull-Clark or Doo-Sabin subdivision. [KP19] argued that bi-4 subdivision rings yields better shape than bi-3 rings but that increment in quality may not be critical when the surrounding surface is a C^1 bi-2 spline. Fig. 4 illustrates that Doo-Sabin subdivision is not useful for most design activities since it generates visible artifacts, e.g. the undue flatness in Fig. 4 b,e. Augmented Subdivision [KP15b] Fig. 4 c,f clearly improves the outcome for convex configurations.

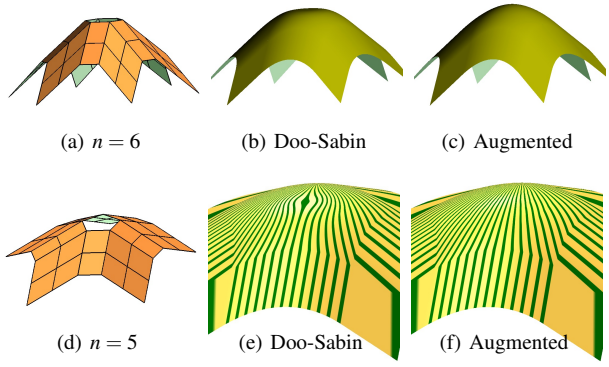

(a) $n=6$ (b) Doo-Sabin (c) Augmented

(d) $n=5$ (e) Doo-Sabin (f) Augmented

Figure 4: *Convex input nets with n-sided central facets surrounded by two layers of quads, the $\overline{DS}$-net. All inner vertices are regular, i.e. have valence* 4. *(a,d) $\overline{DS}$-nets; (e,f) highlight lines [BC94].*

Single-piece, internally C^∞ multi-sided surface caps can be obtained by generalizing transfinite interpolation [VSR12, SVR14, SV18, HK20b, HK20a] or Gregory patches [HK18]. These constructions are controlled by ribbons that define poistion and derivative along boundaries. G-splines [HM90, Pet02] consist of a finite number of polynomial pieces that can yield smooth surfaces by change of variables [LS08, KP16]. As proven in [GP15], and demonstrated in [KNP16, NKP16], G-splines are directly suitable for engineering analysis, but are not well-suited for hierarchical modeling.

To simplify refinability and local geometric editing, hybrid constructions combine a sequence of C^k-joined surface annuli with a tiny n-sided G-spline cap [PK20]. For example, [KP18] yields almost everywhere curvature continuous multi-sided surfaces of degree bi-6. This paper uses the hybrid approach to apply multi-sided caps designed for holes in bi-3 C^2 spline surfaces, but now to holes in a C^1 bi-2 surface. While curvature-bounded guided subdivision [KP19] yields superior shape and fewer surface rings of degree bi-4, we illustrate the approach with the subdivision in [MM18] that generates bi-3 rings of better shape than Catmull-Clark subdivision. The sequence of contracting surface rings is completed by a piecewise polynomial bi-3 geometrically continuous spline cap.

2. The transition from bi-2 to bi-3

This main section briefly reviews standard tools for converting splines and Hermite data to a more local Bernstein-Bézier representation, and then formally define DS-nets and CC-nets shown in Fig. 6 b,e for a pentagonal configuration $n=5$. The goal is to develop formulas to express a CC-net in terms of a DS-net. Since a DS-net has $4n$ points and a CC-net $6n+1$ points this mapping is underconstrained. Functionals fail to usefully pin down the many extra degrees of freedom of the CC-net. Instead we derive explicit formulas that approximate parts of a surface construction, Fig. 2 e. The difference in outcomes, shown in Section 3, motivates this more complex approach over apparently simpler options.

Specifically, we first express a CC-net in terms of a DS-net and a central limit point $\mathbf{Q}$; and then $\mathbf{Q}$ in terms of the DS-net (using the central point of the surface construction [KP21]). This yields a good transition from a DS-net to a CC-net. A reader familiar with the BB-form and not interested in the derivation can skip directly to Equations (3), (4) that summarize the conversion formulas.

Implementation ultimately amounts to a (sparse) matrix multiplication with the input data.

2.1. Conversion from B-spline to BB-form and tensor-borders

Our surfaces are assembled from tensor-product patches of bi-degree d (short bi-d) in Bernstein-Bézier form (BB-form), see e.g. [Far88]:

$$\mathbf{f}(u,v) := \sum_{k=0}^{d}\sum_{\ell=0}^{d} \mathbf{f}_{k\ell} B_k^d(u) B_\ell^d(v), \quad 0 \le u,v \le 1.$$

Here $B_i^d(t) := \binom{d}{i}(1-t)^{d-i}t^i$ are the Bernstein polynomials of degree d and $\mathbf{f}_{ij}$ are the BB-coefficients. Connecting $\mathbf{f}_{ij}$ to $\mathbf{f}_{i+1,j}$ and $\mathbf{f}_{i,j+1}$ wherever possible yields the *BB-net*. Any $(d+1)\times(d+1)$ sub-grid can be interpreted as the control net of a uniform bi-d B-spline. In Fig. 5 the B-spline control points are marked $\circ$. *B-to-BB conversion* expresses the spline in bi-d BB-form illustrated by the green BB-nets in Fig. 5 . For example, applying bi-2 B-to-BB conversion to the $\overline{DS}$-net in Fig. 6 a defines a green ring of bi-2 patches.

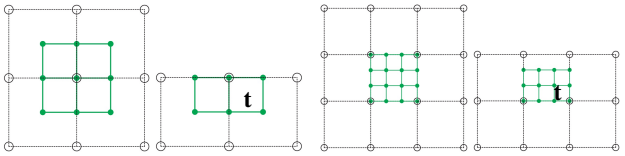

(a) bi-2 B-to-BB conversion (b) bi-3 B-to-BB conversion

Figure 5: *B-to-BB conversion and tensor-borders* $\mathbf{t}$ *as Hermite input data. Circles $\circ$ mark B-spline control points, solid disks $\bullet$ mark BB-coefficients of the full patch, respectively tensor-border.*

Conversion of a partial sub-grid yields a partial BB-net, that defines position and first (and, when $d=3$ possibly second) derivatives across an edge. This representation is called a *tensor-border* and denoted $\mathbf{t}$. Partial conversion of the *DS-net*, the subset of the $\overline{DS}$-net whose nodes marked as $\circ$ in Fig. 6 a,b, yields a first-order

tensor-border ring $\mathbf{t}$, marked green in Fig. 6 b. Partial conversion of the CC-net (nodes marked as • in Fig. 6 d,e) yields a first-order tensor-border ring $\mathbf{t}$, gray underlaid in Fig. 6 d (and a second inner BB-net ring).

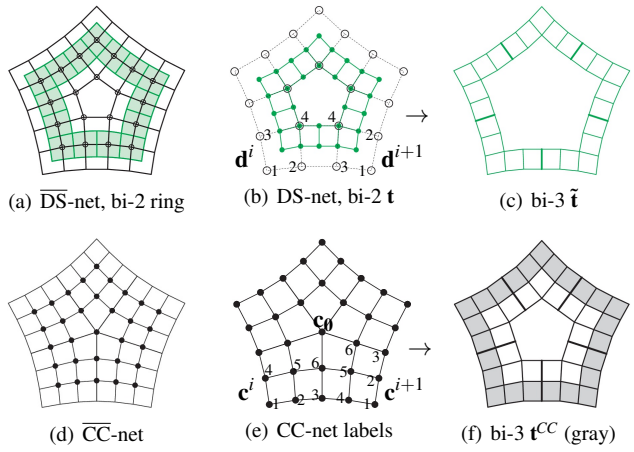

(a) $\overline{\text{DS}}$-net, bi-2 ring (b) DS-net, bi-2 $\mathbf{t}$ (c) bi-3 $\tilde{\mathbf{t}}$

(d) $\overline{\text{CC}}$-net (e) CC-net labels (f) bi-3 $\mathbf{t}^{CC}$ (gray)

Figure 6: *Two ways to generate a degree bi-3 tensor border: top: $\tilde{\mathbf{t}}$ from a DS-net with sector $\mathbf{d}^i$ bottom: $\mathbf{t}^{CC}$ from a CC-net with sector $\mathbf{c}^i$ and n-valent node $\mathbf{c_0}$ ($n=5$).*

2.2. Two ways to compute a central surface point Q

By symbolic computation, the central point $\mathbf{Q}^{KP}$ of the n-sided bi-4 construction [KP21], depicted in Fig. 7 a, can be expressed as weighted sum of the DS-net $\mathbf{d}^j_r$:

$$\mathbf{Q}^{KP} := \kappa_n \sum_{i=0}^{n-1} \mathbf{d}^i_4 + \mu_n \sum_{i=0}^{n-1} (\mathbf{d}^i_2 + \mathbf{d}^i_3) + \nu_n \sum_{i=0}^{n-1} \mathbf{d}^i_1 \,, \qquad (1)$$

where $\nu_n := \frac{1}{n} - \kappa_n - 2\mu_n$, see Fig. 7 b. The labels of $\mathbf{d}$ are displayed in Fig. 6 b. For simplicity and not affecting the final quality, the weights κ_n and μ_n rounded to 5-digits accuracy are

$n=$	3	4	5	6	7	8
$\kappa_n=$	0.29678	0.25	0.21805	0.19282	0.17243	0.15567
$\mu_n=$	0.01887	0	−0.00953	−0.01382	−0.01559	−0.01614

For $n=4$, formula (1) yields, as expected, the quad's centroid, i.e. a corner point of the C^1 bi-2 tensor-product spline.

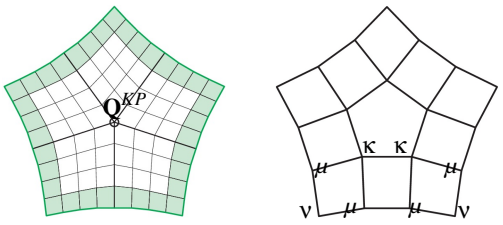

(a) bi-4 cap (b) distribution of κ, μ, ν

Figure 7: *Expressing the center point $\mathbf{Q}^{KP}$ as a weighted sum of a DS-net (with weights κ, μ, ν).*

The central limit point (extraordinary point) $\mathbf{Q}^{CC}$ of Catmull-Clark subdivision [HKD93] for $n>4$ and an improvement for $n=3$ [KP15a] can be expressed in terms of the innermost control nodes of the CC-net:

$$\mathbf{Q}^{CC} := \begin{cases} \frac{n}{n+5}\mathbf{c_0} + \frac{4}{n(n+5)}\sum_{i=0}^{n-1}\mathbf{c}^i_6 + \frac{1}{n(n+5)}\sum_{i=0}^{n-1}\mathbf{c}^i_5, & n>4, \\ \frac{11}{32}\mathbf{c_0} + \frac{1}{6}\sum_{i=0}^{n-1}\mathbf{c}^i_6 + \frac{5}{96}\sum_{i=0}^{n-1}\mathbf{c}^i_5, & n=3. \end{cases} \qquad (2)$$

The labels of $\mathbf{c}$ are displayed in Fig. 6 e.

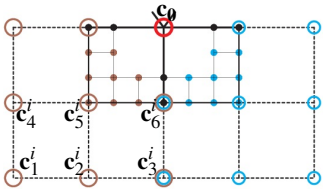

Figure 8: *Tensor-border $\tilde{\mathbf{t}} \Rightarrow$ CC-net.*

2.3. Mapping the DS-net to a CC-net

For each sector (e.g. brown in Fig. 8), reversing the partial B-to-BB conversion maps combinations of $\mathbf{c_0}$ and 8 BB-coefficients of the tensor-border $\tilde{\mathbf{t}}$ (the 8 brown disks • strictly inside the sector) to 8 B-spline CC-net points $\mathbf{c}^i_k$ (marked by brown circles ○). Where CC-net points overlap, e.g. ○ and ○, the average (○ + ○)/2 is retained. This yields

$$\begin{aligned}
\mathbf{c}^i_1 :=& \mathbf{c_0} + \frac{10}{3}\mathbf{d}^i_1 - 2(\mathbf{d}^i_2 + \mathbf{d}^i_3) + \frac{2}{3}\mathbf{d}^i_4 \\
&+ \frac{2}{3}(\mathbf{d}^{i-1}_2 + \mathbf{d}^{i+1}_3) - \frac{2}{3}(\mathbf{d}^{i-1}_4 + \mathbf{d}^{i+1}_4)\,, \\
\mathbf{c}^i_2 :=& -\frac{1}{2}\mathbf{c_0} + \frac{5}{8}\mathbf{d}^i_1 + \frac{35}{24}\mathbf{d}^i_2 - \frac{11}{4}\mathbf{d}^i_3 - \frac{5}{8}\mathbf{d}^i_4 \\
&+ \frac{1}{12}\mathbf{d}^{i-1}_2 + \frac{5}{12}\mathbf{d}^{i-1}_4 - \frac{1}{3}\mathbf{d}^{i+1}_3 + \frac{1}{3}\mathbf{d}^{i+1}_4\,, \\
\mathbf{c}^i_4 :=& -\frac{1}{2}\mathbf{c_0} + \frac{5}{8}\mathbf{d}^i_1 + \frac{35}{24}\mathbf{d}^i_3 - \frac{11}{4}\mathbf{d}^i_2 - \frac{5}{8}\mathbf{d}^i_4 \\
&+ \frac{1}{12}\mathbf{d}^{i+1}_3 + \frac{5}{12}\mathbf{d}^{i+1}_4 - \frac{1}{3}\mathbf{d}^{i-1}_2 + \frac{1}{3}\mathbf{d}^{i-1}_4\,, \\
\mathbf{c}^i_5 :=& \frac{1}{4}\mathbf{c_0} + \frac{5}{48}\mathbf{d}^i_1 + \frac{5}{16}(\mathbf{d}^i_2 + \mathbf{d}^i_3) + \frac{25}{48}\mathbf{d}^i_4 \\
&- \frac{1}{24}(\mathbf{d}^{i-1}_2 + \mathbf{d}^{i+1}_3) - \frac{5}{24}(\mathbf{d}^{i-1}_4 + \mathbf{d}^{i+1}_4)\,, \\
\mathbf{c}^i_3 :=& \mathbf{c_0} - \frac{1}{6}(\mathbf{d}^i_1 + \mathbf{d}^{i+1}_1) + \frac{7}{6}(\mathbf{d}^i_2 + \mathbf{d}^{i+1}_3) \\
&+ \frac{1}{6}(\mathbf{d}^i_3 + \mathbf{d}^{i+1}_2) - \frac{7}{6}(\mathbf{d}^i_4 + \mathbf{d}^{i+1}_4)\,, \\
\mathbf{c}^i_6 :=& -\frac{1}{2}\mathbf{c_0} - \frac{1}{48}(\mathbf{d}^i_1 + \mathbf{d}^{i+1}_1) + \frac{7}{48}(\mathbf{d}^i_2 + \mathbf{d}^{i+1}_3) \\
&- \frac{5}{48}(\mathbf{d}^i_3 + \mathbf{d}^{i+1}_2) + \frac{35}{48}(\mathbf{d}^i_4 + \mathbf{d}^{i+1}_4)\,.
\end{aligned} \qquad (3)$$

Substituting $\mathbf{c}^i_5$ and $\mathbf{c}^i_6$ into (2) and setting $\mathbf{Q}^{CC} := \mathbf{Q}^{KP}$ yields

$$\mathbf{c_0} := \begin{cases} \frac{16n(n+5)\mathbf{Q}^{KP} + \sum_{i=0}^{n-1}\left(\mathbf{d}^i_1 - 7(\mathbf{d}^i_2 + \mathbf{d}^i_3) - 95\mathbf{d}^i_4\right)}{4n(4n-7)}, & n>4; \\ \frac{4608\mathbf{Q}^{KP} + \sum_{i=0}^{n-1}\left(7\mathbf{d}^i_1 - 97(\mathbf{d}^i_2 + \mathbf{d}^i_3) - 1145\mathbf{d}^i_4\right)}{612}, & n=3. \end{cases} \qquad (4)$$

That is, we expressed the CC-net in terms of the DS-net see Fig. 6 b,e.

2.4. The transition ring

We now construct a smooth bi-3 transition surface ring that connects to the bi-2 data on the outside and a multi-sided cap on the inside. Due to the different requirements of [CC78] and [MM18] we need to discuss two options.

See Fig. 9 . B-to-BB conversion of a $\overline{\text{CC}}$-net (a) yields a sector of a bi-3 ring in BB-form, colored orange in (b). Catmull-Clark refinement of the same $\overline{\text{CC}}$-net yields the $\overline{\text{CC}}$-net of the next step. Following the ⇓ in Fig. 9 , refining the $\overline{\text{CC}}$-net by the rules of [MM18] (d) and subsequent B-to-BB conversion yields two bi-3 rings in (e) and a subset of the refined net (d) forms the $\overline{\text{CC}}$-net for the next step (f). The two $\overline{\text{CC}}$-nets (c) and (f) differ in the control points marked by □, nearest to the extraordinary point.

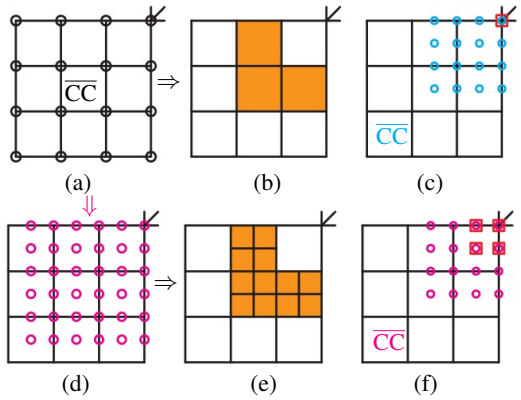

Figure 9: *Refinement creating top: a single width bi-3 Catmull-Clark ring or bottom: a double width bi-3 curvature-bounded subdivision ring [MM18].*

We first apply one Catmull-Clark step to the CC-net $\mathbf{c}$ computed in the previous sections and retain the $\overline{\text{CC}}$-net as Fig. 10 a whose sector is shown in Fig. 9 c. (For $n = 3$, best shape is obtained by using, only in the first step, the Catmull-Clark weights [PR08] $\alpha = 3/8, \beta = 1/2$). This yields the $n \times 3$ patch structure and layout of Catmull-Clark subdivision. To obtain the structure and layout required by [MM18], namely $n \times 12$patches, the refinement Fig. 9 a to Fig. 9 c is applied a second time followed by (d) to (f).

Fig. 10 shows once more the BB-nets of the transition ring. The outer bi-2 patches are indicated as dark green stripes to the lower left and the location of the multi-sided surface cap is indicated to the upper right in light-red. The two-sided Hermite extension of Fig. 10 yields a transition ring that is connected C^1 to both the outer input bi-2 data and inner multi-sided surface cap.

3. Central cap, Examples and Discussion

To avoid infinite recursion and because no higher refinement level is expected, the rings generated by the subdivision algorithms are filled with a tiny central cap. All examples use this practical finite completion.

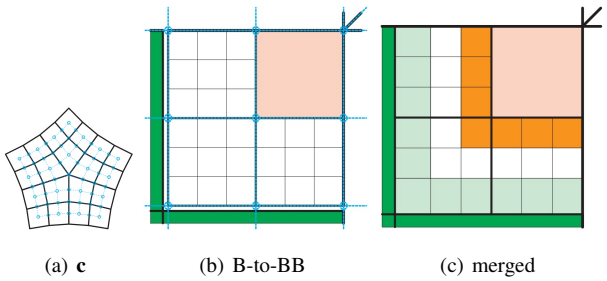

Figure 10: *BB-net of the transition ring. (a) CC-net* $\mathbf{c}(\mathbf{d})$ *and its refinement* $\overline{\text{CC}}$*-net (partly concealed by the black edges of* $\mathbf{c}(\mathbf{d})$*, enlarge) by one Catmull-Clark step. (b) One sector of B-to-BB conversion of the* $\overline{\text{CC}}$*-net, cf. Fig. 9 b. (c) Extending with first-order Hermite data from the surrounding bi-2 spline (light-green) and from the cap (orange).*

3.1. The tiny cap of degree bi-3

To preserve the surface quality and keep the degree bi-3, we mimic the approach of [KP15a] and connect a G^1 cap consisting of n bi-3 macro-patches formally only C^0 to the last subdivision ring, but with a normal deviation of typically $< 0.1^o$. Such tolerances are accepted in industrial class A surface construction as long as the highlight line distribution is uniform [Aut15]. Conversely, all known truly smooth bi-3 caps yield clearly worse highlight line distributions. (An extended version of this paper will include a second Appendix describing a new, formally smoothly-joined bi-3 cap with good highlight lines).

3.2. Examples

We first test the approach on the trivial configuration, $n = 4$. The choice $\kappa_4 := \frac{1}{4}$, $\mu_4 := 0$ in formula (1) selects the centroid of the central face as $\mathbf{Q}$ when deriving $\mathbf{c}(\mathbf{d})$. Fig. 11 demonstrates that this choice works well. When $n \neq 4$, choosing $\mathbf{Q}$ as the centroid of central face yields poor shape and (2) must be used instead: for $n = 3$, Fig. 12 , choosing $\mathbf{Q}$ to be the centroid results in too-pointed a surface (as is evident from the pinched highlight lines in Fig. 12 c) – whereas for $n = 5$, choosing $\mathbf{Q}$ to be the centroid results in flatness (spread out highlight lines in Fig. 13 c). This is akin to the shape deficiencies of Doo-Sabin subdivision, which considers only the central face, compared to Augmented Subdivision, which looks beyond that face.

Applying one Catmull-Clark step to the $\overline{\text{DS}}$-net is another obvious choice to generate a CC-net. Fig. 13 e confirms that this naive approach creates unacceptable surface shape, visible even without highlight lines. The underlying reason can be understood via the curve case Fig. 13 f: starting with a near-circular loop of degree 2, *left*, the top segment is treated like the n-sided face of a DS-net: midpoint knot insertion for cubic splines plays the role of one Catmull-Clark step and the points marked ∘ form the CC-net, *middle*. Two C^2-connected cubics (blue, *right*) mimic the subdivision rings of [MM18], whereas the cyan cubics (obtained by C^1 extension of the green quadratic and blue cubic curves) mimic the tran-

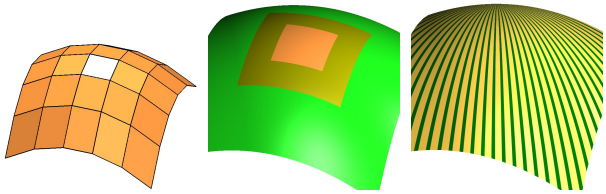

(a) $n = 4$ $\overline{\text{DS}}$-net (b) layout (c) highlight lines

Figure 11: *Convex $\overline{DS}$-net to test the trivial case $n = 4$. (b) The transition ring is bronze. The central orange surface cap consists of four bi-3 patches.*

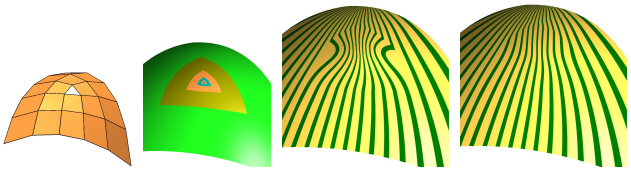

(a) $n = 3$ (b) layout (c) centroid (d) default $\mathbf{Q}$

Figure 12: *(a) Convex $\overline{DS}$-net, $n = 3$. The surface rings consists of n bi-3 patches per sector. The first refinement Fig. 9 $a \to c$ uses the non- standard Catmull-Clark weightings $\alpha = 3/8$, $\beta = 1/2$.*

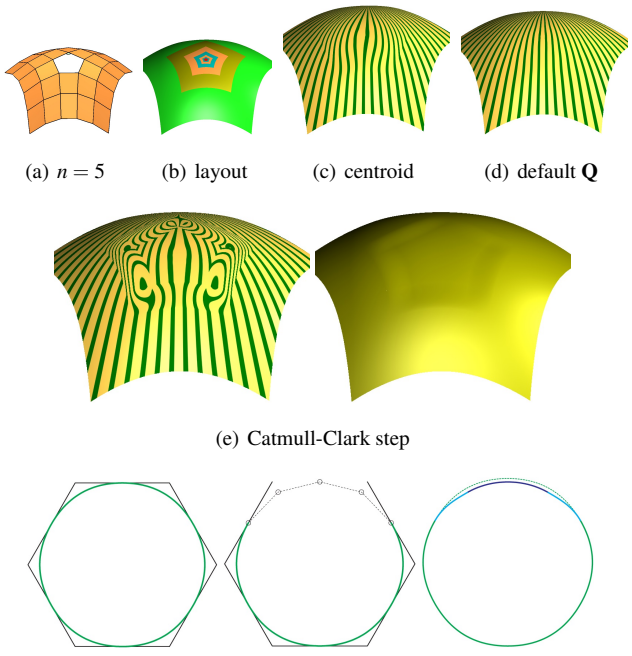

(a) $n = 5$ (b) layout (c) centroid (d) default $\mathbf{Q}$

(e) Catmull-Clark step

(f) naive approach illustrated for curves

Figure 13: *Convex $\overline{DS}$-net, $n = 5$. (b) The transition rings consist of a single layer (three bi-3 patches per sector). (c),(d) motivate the default choice of $\mathbf{Q}$. (f) is the curve analogue to (e) predicting the failure of the naive construction of a transition in (e).*

sition ring. Compared to the original quadratic (dashed green) the flatness of the naive construction is evident.

Fig. 14 for $n = 7$ and Fig. 14 for $n = 8$ compare rings generated by [MM18], (b,d) with the more sophisticated approach of guided subdivision (c,f). Guided subdivision allows doubling the contraction speed so that fewer rings (c) vs (b) are needed to reach the tiny cap. Guided subdivision also joins transition and cap better than does [MM18]. However, the main body is bi-4 rather than bi-3.

4. Conclusion

A new surface transition ring allows filling multi-sided holes in C^1 bi-2 splines with well-known subdivision algorithms. We looked at Catmull-Clark, a curvature-bounded and guided subdivision. Depending on the choice of algorithm, the multi-sided surface cap is of moderate to high quality as measured in terms of the highlight line distribution, and implementation is of moderate to high complexity. We also proposed to use only a few subdivision rings and complete the multi-sided surface with a tiny bi-cubic cap so that, for example, a few steps of the curvature-bounded algorithm yield a finite bi-cubic multi-sided surface. This is analogous to [KP21], but replaces the guide surface construction and application by the short, explicit formulas (3) and (4) that express a CC-(control-)net in terms of a DS-net.

Notably, the formulas were obtained by applying a surface construction symbolically rather than numerically. Ultimately, the construction amounts to multiplication of the DS-net with a pre-computed matrix. More generally, to construct surfaces from a polyhedral net, the CC-net can be derived from an arbitrary bi-3 tensor-borders $\tilde{\mathbf{t}}$, not just to those defined by a DS-net.

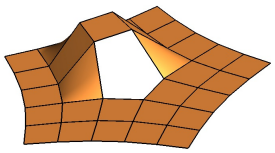

Figure 15: *Challenging input net that can motivate more complex formulas*

The goal was to keep the formulas simple. A more complex formula for $\mathbf{c}_5^i$ and $\mathbf{c}_6^i$ can be used to improve the shape of difficult configurations like Fig. 15 where one part of the otherwise planar net has been lifted up. However for most common cases, the examples showed that the construction avoids major shape deficiencies that simpler and at first glance natural constructions are prone to.

Acknowledgements This work was supported in part by DARPA HR00111720031 and NIH R01 EB018625

References

[Aut15] AUTODESK: Tutorial at http://help.autodesk.com/view/alias/2015/enu/?guid=guid-2fce06eb-8ef7-4507-92f7-82a73a0df378, 2015. accessed Jan 16. 5

[BC94] BEIER K.-P., CHEN Y.: Highlight-line algorithm for realtime surface-quality assessment. *Comp-Aid Design 26*, 4 (1994), 268–277. 1, 2, 3

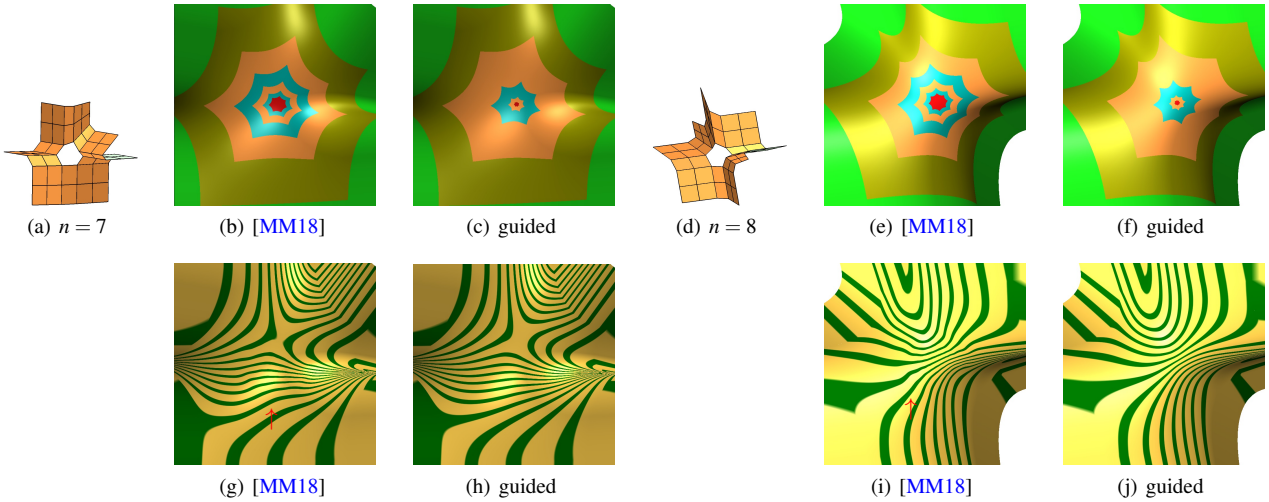

(a) $n = 7$ (b) [MM18] (c) guided (d) $n = 8$ (e) [MM18] (f) guided

(g) [MM18] (h) guided (i) [MM18] (j) guided

Figure 14: *Surface caps for $n = 7$ and $n = 8$. (b,e) Sequence of C^2-joined rings according to [MM18]. (d,f) Sequence of C^1-joined rings according to guided subdivision [KP19].*

[CADS09] CASHMAN T. J., AUGSDÖRFER U. H., DODGSON N. A., SABIN M. A.: NURBS with extraordinary points: high-degree, non-uniform, rational subdivision schemes. *ACM Tr Graph 28*, 3 (2009), 46:1–46:9. 3

[CC78] CATMULL E., CLARK J.: Recursively generated B-spline surfaces on arbitrary topological meshes. *Computer-Aided Design 10* (Sept. 1978), 350–355. 1, 2, 5

[DS78] DOO D., SABIN M.: Behaviour of recursive division surfaces near extraordinary points. *Computer-Aided Design 10* (Sept. 1978), 356–360. 1, 2

[Far88] FARIN G.: *Curves and Surfaces for Computer Aided Geometric Design: A Practical Guide*. Academic Press, 1988. 3

[GP15] GROISSER D., PETERS J.: Matched G^k-constructions always yield C^k-continuous isogeometric elements. *Computer Aided Geometric Design 34* (March 2015), 67–72. 3

[HK18] HETTINGA G. J., KOSINKA J.: Multisided generalisations of Gregory patches. *Computer Aided Geometric Design 62* (2018), 166–180. 3

[HK20a] HETTINGA G. J., KOSINKA J.: Multisided B-spline Patches Over Extraordinary Regions. In *Smart Tools and Apps for Graphics - Eurographics Italian Chapter Conference* (2020), Biasotti S., Pintus R., Berretti S., (Eds.), The Eurographics Association. 3

[HK20b] HETTINGA G. J., KOSINKA J.: A multisided C^2 B-spline patch over extraordinary vertices in quadrilateral meshes. *Comput. Aided Des 127* (2020), 102855. 3

[HKD93] HALSTEAD M., KASS M., DEROSE T.: Efficient, fair interpolation using catmull-clark surfaces. 35–44. 4

[HM90] HÖLLIG K., MÖGERLE H.: G-splines. *Computer-Aided Geometric Design 7* (1990), 197–207. 3

[KNP16] KARČIAUSKAS K., NGUYEN T., PETERS J.: Generalizing bicubic splines for modelling and IGA with irregular layout. *Computer Aided Design 70* (Jan 2016), 23–35. 3

[KP07] KARČIAUSKAS K., PETERS J.: Concentric tesselation maps and curvature continuous guided surfaces. *Computer Aided Geometric Design 24*, 2 (Feb 2007), 99–111. 3

[KP15a] KARČIAUSKAS K., PETERS J.: Can bi-cubic surfaces be class A? *Computer Graphics Forum 34*, 5 (August 2015), 229–238. 4, 5

[KP15b] KARČIAUSKAS K., PETERS J.: Point-augmented biquadratic C^1 subdivision surfaces. *Graphical Models 77* (Jan 2015), 18–26. 1, 3

[KP16] KARČIAUSKAS K., PETERS J.: Minimal bi-6 G^2 completion of bicubic spline surfaces. *Computer Aided Geometric Design 41* (Jan 2016), 10–22. 3

[KP18] KARČIAUSKAS K., PETERS J.: Fair free-form surfaces that are almost everywhere parametrically C^2. *Journal of Computational and Applied Mathematics* (2018), 1–10. 3

[KP19] KARČIAUSKAS K., PETERS J.: Curvature-bounded guided subdivision: biquartics vs bicubics. *Computer Aided Design* (Jul 2019), 1–11. 2, 3, 7

[KP21] KARČIAUSKAS K., PETERS J.: Least degree G^1-refinable multi-sided surfaces suitable for inclusion into C^1 bi-2 splines. *Computer-Aided Design 130* (2021), 1–12. 1, 2, 3, 4, 6

[KPR04] KARCIAUSKAS K., PETERS J., REIF U.: Shape characterization of subdivision surfaces – case studies. *Computer-Aided Geometric Design 21*, 6 (july 2004), 601–614. 3

[LFS16] LI X., FINNIGAN G., SEDERBERG T.: G^1 non-uniform Catmull-Clark surfaces. *ACM Transactions on Graphics 35* (07 2016), 1–8. 3

[LS08] LOOP C. T., SCHAEFER S.: G^2 tensor product splines over extraordinary vertices. *Comput. Graph. Forum 27*, 5 (2008), 1373–1382. 3

[MM18] MA Y., MA W.: Subdivision schemes with optimal bounded curvature near extraordinary vertices. *Computer Graphics Forum 37*, 7 (Oct 2018), 455–467. 2, 3, 5, 6, 7

[NKP16] NGUYEN T., KARČIAUSKAS K., PETERS J.: C^1 finite elements on non-tensor-product 2d and 3d manifolds. *Applied Mathematics and Computation 272*, 1 (2016), 148–158. 3

[Pet02] PETERS J.: Geometric continuity. In *Handbook of Computer Aided Geometric Design* (2002), Elsevier, pp. 193–229. 3

[PK20] PETERS J., KARČIAUSKAS K.: Subdivision and G-spline hybrid constructions for high-quality geometric and analysis-suitable surfaces. In *Geometric Challenges in Isogeometric Analysis* (2020), Carla Manni H. S., (Ed.), vol. to appear, Istituto Nazionale di Alta Matematica Francesco Severi (INdAM), pp. 1–15. Springer INdAM. 3

[PR08] PETERS J., REIF U.: *Subdivision Surfaces*, vol. 3 of *Geometry and Computing*. Springer-Verlag, New York, 2008. 5

[SV18] SALVI P., VÁRADY T.: Multi-sided Bézier surfaces over concave polygonal domains. *Comput. Graph 74* (2018), 56–65. 3

[SVR14] SALVI P., VÁRADY T., ROCKWOOD A. P.: Ribbon-based transfinite surfaces. *Comput. Aided Geom. Des 31*, 9 (2014), 613–630. 3

[TSHH17] TOSHNIWAL D., SPELEERS H., HIEMSTRA R., HUGHES T.: Multi-degree smooth polar splines: A framework for geometric modeling and isogeometric analysis. *Computer Methods in Applied Mechanics and Engineering 316* (2017), 1005–1061. 3

[VSR12] VÁRADY T., SALVI P., ROCKWOOD A. P.: Transfinite surface interpolation with interior control. *Graph. Model 74*, 6 (2012), 311–320. 3